THE JOURNAL OF BIOLOGICAL CHEMISTRY
Vol. 279, No. 30, Issue of July 23, pp. 31655–31663, 2004
Printed in U.S.A.

Structural Basis for the Autoinhibition and STI-571 Inhibition of c-Kit Tyrosine Kinase*

Received for publication, March 25, 2004, and in revised form, April 29, 2004
Published, JBC Papers in Press, April 29, 2004, DOI 10.1074/jbc.M403319200

Clifford D. Mol‡§, Douglas R. Dougan‡, Thomas R. Schneider¶, Robert J. Skene‡, Michelle L. Kraus‡, Daniel N. Scheibe‡, Gyorgy P. Snell‡, Hua Zou‡, Bi-Ching Sang‡, and Keith P. Wilson‡

From ‡Syrrx, Inc., San Diego, California, 92121 and the ¶Italian Foundation of Cancer Research (FIRC) Institute of Molecular Oncology, Via Adamello, 16 Milan, Italy, 20139

The activity of the c-Kit receptor protein-tyrosine kinase is tightly regulated in normal cells, whereas deregulated c-Kit kinase activity is implicated in the pathogenesis of human cancers. The c-Kit juxtamembrane region is known to have an autoinhibitory function; however the precise mechanism by which c-Kit is maintained in an autoinhibited state is not known. We report the 1.9-Å resolution crystal structure of native c-Kit kinase in an autoinhibited conformation and compare it with active c-Kit kinase. Autoinhibited c-Kit is stabilized by the juxtamembrane domain, which inserts into the kinase-active site and disrupts formation of the activated structure. A 1.6-Å crystal structure of c-Kit in complex with STI-571 (Imatinib® or Gleevec®) demonstrates that inhibitor binding disrupts this natural mechanism for maintaining c-Kit in an autoinhibited state. Together, these results provide a structural basis for understanding c-Kit kinase autoinhibition and will facilitate the structure-guided design of specific inhibitors that target the activated and autoinhibited conformations of c-Kit kinase.

The stem cell factor receptor c-Kit is a receptor protein-tyrosine kinase (RPTK)[1] that initiates cell growth and proliferation signal transduction cascades in response to stem cell factor binding (1). c-Kit, named after its viral homolog v-Kit (2), is a member of the Type III transmembrane RPTK subfamily, which includes the colony-stimulating factor-1 receptor (3), also known as the FMS receptor, the related Flt-3 receptor (4), and the platelet-derived growth factor α- and β-receptors (5, 6), as well as c-Kit (7). The Type III RPTK family is characterized by five extracellular immunoglobulin (Ig) domains, a single transmembrane helix, an autoinhibitory juxtamembrane domain, and a cytoplasmic kinase domain that is split by a kinase insertion domain (KID) (see Fig. 1*A*) (6, 8).

The binding of a stem cell factor dimer to the extracellular Ig domains of c-Kit causes two c-Kit RPTKs to dimerize and permits the kinase domains to act in *trans* as a substrate and enzyme for one another. The result of stem cell factor binding is the phosphorylation of specific tyrosine residues located in c-Kit juxtamembrane regions (9–12). Tyrosine residue 568 is the primary site of *in vivo* autophosphorylation (see Fig. 1*B*). Phosphorylation of the tyrosine initiates a cytoplasmic serine/threonine phosphorylation cascade that promotes cell growth and proliferation (12). Mutations that cause constitutive activation of c-Kit kinase activity in the absence of stem cell factor binding are implicated in highly malignant human cancers, including gastrointestinal stromal tumors (13, 14), germ cell tumors (15), mast cell and myeloid leukemias (16), and in mastocytosis (17). Moreover, activating c-Kit mutations that occur in the kinase domain are resistant to many kinase inhibitors currently in use as chemotherapy treatments (18–21).

The kinase activity of c-Kit is tightly regulated throughout its signaling cycle. Binding of the protein-tyrosine phosphatase SHP-1 to the phosphorylated c-Kit juxtamembrane region results in dephosphorylation of the tyrosine residues and termination of the intracellular signal (22). The dual role of the juxtamembrane region as an unphosphorylated autoinhibitory domain and as a phosphorylated intracellular signal has made it difficult to dissect the structural and mechanistic functions of the juxtamembrane region in the signaling cascade. Specific site-directed mutations introduced into the juxtamembrane domains of c-Kit (23) and platelet-derived growth factor (24, 25) indicate that several residues are necessary to maintain the kinase in an autoinhibited state (see Fig. 1*B*). Based on amino acid sequence analysis the Type III RPTK juxtamembrane domains are proposed to adopt a conformation similar to WW domains, which are implicated in regulating cellular processes (26–28). Similarly, the c-Kit autoinhibitory juxtamembrane region has been proposed to form a putative α-helix that exerts negative control over uninduced receptor (23). Studies with a synthetic peptide of the c-Kit juxtamembrane region suggest that it folds as an autonomous domain and directly interacts with the amino-terminal lobe of the kinase domain (29).

These models for the autoinhibition of Type III RPTKs are derived from autoregulation mechanisms inferred from the crystal structures of other protein-tyrosine kinases (reviewed in Refs. 30 and 31). Autoinhibition in *cis* is seen in the crystal structure of the autoinhibited form of the EphB2 receptor tyrosine kinase domain (32). This structure contains a truncated juxtamembrane domain with phenylalanine substitution mutations of signaling tyrosine residues similar to those in the juxtamembrane regions of c-Kit and the Type III RPTKs. The visible portion of the EphB2 juxtamembrane domain forms a short α-helix that packs against the amino-terminal lobe of the kinase and disrupts the interactions of the control, or C, helix

* The costs of publication of this article were defrayed in part by the payment of page charges. This article must therefore be hereby marked "*advertisement*" in accordance with 18 U.S.C. Section 1734 solely to indicate this fact.

The atomic coordinates and structure factors (codes 1T45 and 1T46) have been deposited in the Protein Data Bank, Research Collaboratory for Structural Bioinformatics, Rutgers University, New Brunswick, NJ (http://www.rcsb.org/).

§ To whom correspondence should be addressed. E-mail: clifford.mol@syrrx.com.

[1] The abbreviations used are: RPTK, receptor protein-tyrosine kinase; KID, kinase insertion domain; MuSK, autoinhibited muscle-specific kinase; MES, 4-morpholineethanesulfonic acid; PTR, phosphotyrosine; SH, Src homolgy; RMS, root mean square.

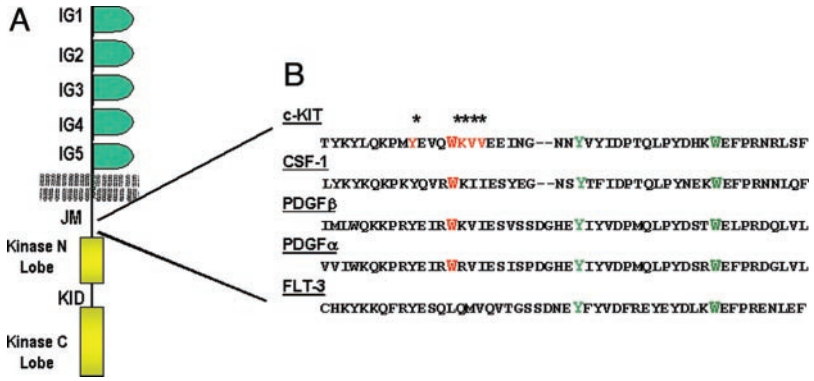

FIG. 1. **Gene organization and juxtamembrane domain sequence conservation of the Type III receptor RPTK.** *A*, schematic diagram of the Type III RPTK gene/protein organization showing the five extracellular immunoglobulin (*IG*) domains, the cell membrane, and membrane-spanning segment, the juxtamembrane (*JM*) region, and the intracellular c-Kit kinases domains separated by the kinase insertion domain (*KID*). *B*, sequence alignment of the juxtamembrane regions of the Type III RPTKs. The putative WW-like domain residues Trp^{557} and Trp^{580} (c-Kit numbering) are shown in *red* and *green*, respectively. Trp^{580} marks the beginning of the formal kinase domains. Tyr^{568}, the target for *trans* phosphorylation, is shown in *aqua*. *Asterisks* denote residues in which the mutation in c-Kit increases basal receptor phosphorylation (Ma *et al.*, Ref. 23).

TABLE I
X-ray data collection and refinement statistics

	Autoinhibited	Activated	STI-571
Data collection			
Resolution (Å)	30.0–1.90 (1.97–1.90)	30.0–2.65 (2.74–2.65)	30.0–1.60 (1.66–1.60)
Observations	107,299	98,443	220,014
Unique reflections	26,260	21,243	48,006
Completeness (%)	98.3 (96.5)	99.3 (95.1)	98.4 (90.0)
$I/\sigma I$	12.6 (3.1)	15.4 (2.0)	19.3 (2.6)
R_{sym} [a]	0.058 (0.345)	0.046 (0.493)	0.028 (0.367)
Refinement			
Resolution (Å)	20.0–1.90	10.0–2.65	20.0–1.60
Reflections used	24,835	19,687	45,483
Number of protein atoms	2,689	4,672	2,381
Number of ligand atoms	0	57	37
Number of solvent atoms	208	23	268
RMS bonds (Å)	0.009	0.012	0.007
RMS angles (°)	1.112	1.335	1.085
Average B-value (Å^2)	16.9	54.9	23.6
R-value, R_{free} [b]	0.193, 0.222	0.223, 0.276	0.188, 0.213

[a] $R_{sym} = \Sigma_h \Sigma_j |\langle I(h)\rangle - I(h)j| / \Sigma_h \Sigma_j \langle I(h)\rangle$ where $\langle I(h)\rangle$ is the mean intensity of symmetry-related reflections.
[b] R-value $= \Sigma ||F_{obs}| - |F_{calc}|| / \Sigma |F_{obs}|$; R_{free} for 5% of reflections excluded from refinement. Values in parentheses are for the respective high resolution shells.

with residues that form an activated kinase ATP-binding site. Similarly, the crystal structure of the autoinhibited muscle-specific kinase MuSK reveals a small ordered segment of the MuSK juxtamembrane region that forms a short α-helix, which likely impedes the ability of the C-helix to contribute to productive binding of ATP (33). An autoinhibitory structural role for a juxtamembrane region tyrosine residue was also inferred from the crystal structure of the insulin receptor in which a similar disruption of the conformation of the C-helix was observed (34).

Targeting these distinct inactive kinase conformations for a rational drug design may allow for the design of tight binding and specific compounds. STI-571, also known as Imatinib® or Glivec®/Gleevec®, is one such drug compound that specifically binds to the inactive conformation of the Abl kinase. Abl kinase is directly implicated in the pathogenesis of chronic myelogenous leukemia (35). Notably, STI-571 does not inhibit many other kinases, but it does inhibit the two closely related Type III RPTKs, platelet-derived growth factor and c-Kit (36). Recently we reported (37) the 2.9-Å resolution crystal structure of an activated c-Kit kinase domain-product complex bound in *trans* with juxtamembrane phosphotyrosine residues and ADP and Mg^{2+}. For comparative analysis, we recapitulate that structure here at an improved 2.65-Å resolution. We also present the 1.9-Å resolution crystal structure of unphosphorylated c-Kit kinase containing the entire autoinhibitory juxtamembrane region. The juxtamembrane domain inserts directly into the cleft between the kinase amino- and carboxyl-terminal lobes, disrupting the c-Kit control helix, and physically blocking the conserved kinase Asp-Phe-Gly (DFG) motif from attaining a productive conformation. The kinase activation loop folds back over the substrate-binding groove and interacts with the kinase-active center as a pseudosubstrate. We also present a 1.6-Å resolution co-crystal structure of a c-Kit·STI-571 complex that illustrates that portions of the inhibitor would clash with regions of the juxtamembrane domain that maintain c-Kit in the autoinhibited conformation. These results provide the detailed molecular basis for understanding the mechanism of c-Kit kinase autoinhibition and will facilitate the structure-guided design of specific and potent inhibitors that target the activated and autoinhibited conformations of c-Kit kinase.

EXPERIMENTAL PROCEDURES

Protein Expression and Purification—The portion of the human *c-Kit* gene that comprises the catalytic kinase domains and the entire intact juxtamembrane domain (residues 544–935, GenBank™ accession number NM_000222 (3)) with the KID residues 694–753 deleted was cloned and expressed as described previously (37). Recombinant c-Kit protein was expressed in *Spodoptera frugiperda* cells in 5L Wave Bio-Reactors with ESF-921 protein-free media (Expression Systems), and the cells were harvested after 2 days. The protein yield was 3.77

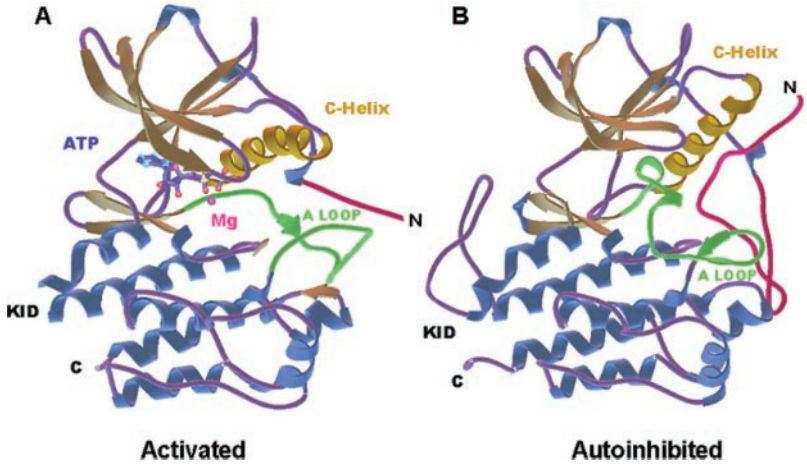

FIG. 2. **Overall structures of activated and autoinhibited c-Kit kinase.** *A*, a Cα ribbon diagram of active c-Kit kinase showing the positions of the N and C termini and the location of the kinase insertion domain (*KID*), with α-helices (*blue*), β-strands (*amber*), and loops (*purple*). The kinase-active center is illustrated by the bound ADP (*blue*) and Mg^{2+} ion (*pink*). The C-helix (*gold*) is in a productive orientation and the A-loop (*green*) is in an extended conformation. The substrate-peptide portion of the amino-terminal juxtamembrane domain (*purple*) extends from the main body of the kinase and is bound in *trans* to a second molecule in the crystal lattice. *B*, a Cα ribbon diagram of the autoinhibited c-Kit kinase with protein secondary structure elements, C-helix, A-loop, and amino-terminal juxtamembrane domain colored as in *A*. The entire juxtamembrane region is visible in this structure and inserts between the kinase N- and C-lobes, shifting the position of the C-helix, and sterically blocking the A-loop from attaining its extended active conformation. The autoinhibited A-loop folds back over the kinase C-Lobe and binds as a pseudosubstrate.

mg/liter and the recombinant protein, containing an amino-terminal His_6 tag followed by an rTEV protease cleavage site, was purified by Ni^{2+}-chelate chromatography, the tag was removed with rTEV protease, and the tag and any uncleaved material were removed by a second passage over a ProBond Ni^{2+}-chelate column. Purified c-Kit protein was judged to be >95% pure by SDS-PAGE and was concentrated to 6–12 mg/ml in buffer containing 25 mM Tris, pH 7.6, 250 mM NaCl, 5 mM dithiothreitol, and 1 mM EDTA. Purified and concentrated c-Kit protein was flash-frozen in 50-μl aliquots by direct immersion in liquid nitrogen and stored at −80 °C.

Crystallization and Data Collection—Crystals of activated c-Kit kinase domain (~0.2 × 0.2 × 0.05 mm) are grown at 20 °C as described (37) by pre-incubating enzyme samples (6 mg/ml) with ATP and $MgCl_2$ prior to performing sitting-drop crystallization experiments using 5 μl of protein solution and 5 μl of reservoir solution (18% polyethylene glycol 8000, 0.1 M MES, pH 7.1). Crystals of autoinhibited c-Kit kinase (~0.1 × 0.1 × 0.2 mm) are obtained at 20 °C from the same protein preparation (10 mg/ml) using Nanovolume Crystallization® (38) techniques with 50 nl of protein solution and 50 nl of reservoir solution containing 13% polyethylene glycol 8000, 0.1 M HEPES, pH 7.0. For crystals of the co-complex with STI-571 (~0.1 × 0.1 × 0.1 mm), 50 nl of enzyme-inhibitor solution and 50 nl of reservoir (2 M phosphate, 0.1 M Tris, pH 8.5) were used, and the crystals were grown at 4 °C. Single crystals of all enzyme forms were harvested in reservoir solutions supplemented with 25% ethylene glycol, and flash-frozen by direct immersion in liquid nitrogen. X-ray diffraction data were collected at the Advanced Light Source Beam Line 5.0.3 equipped with an ADSC Quantum4 CCD detector, and the diffraction intensities were integrated and scaled using the HKL2000 program suite (39). The activated c-Kit kinase crystals belong to the orthorhombic space group $P2_12_12$ with unit cell dimensions a = 95.3 Å, b = 119.5 Å, and c = 62.6Å and contain two enzyme molecules in the asymmetric unit. The autoinhibited c-Kit kinase crystals belong to the orthorhombic space group $P2_12_12_1$ with unit cell dimensions a = 44.4 Å, b = 77.2 Å, and c = 94.6 Å and possess one enzyme molecule in the asymmetric unit. The c-Kit·STI-571 complex crystals are in the trigonal space group $P3_221$ with unit cell dimensions $a = b$ = 70.1 Å and c = 127.9 Å and contain one enzyme-inhibitor co-complex in the asymmetric unit.

Structure Determination and Refinement—The structure of activated c-Kit kinase was determined by molecular replacement using AMoRe (40) and refined as described previously (37). This structure contains two c-Kit enzyme molecules in the asymmetric unit and clear electron density for residues 567–935 of both enzymes, with the exception of ~20 amino-terminal amino acid residues as well as ~10 residues comprising the truncated KID, which are disordered. The structure of autoinhibited c-Kit kinase contains only one enzyme molecule in the asymmetric unit and was also determined by molecular replacement with AMoRe, using the activated c-Kit kinase structure as a search model with the correct solution yielding a correlation coefficient of 0.30 and an initial R-value of 0.50. The initial solutions were refined with REFMAC (41), and the models were visually inspected and manually built and rebuilt using the XtalView/Xfit program suite (42). The structure of autoinhibited c-Kit kinase is fully ordered with unambiguous electron density for residues 548–935, including the truncated KID residues. For the structure of the c-Kit·STI-571 complex two molecular replacement calculations were performed utilizing the activated structure (correlation coefficient 0.28, R-value 0.47) and the autoinhibited structure (correlation coefficient 0.39, R-value 0.44). The autoinhibited structure was clearly the better model, and a refinement of this model yielded clear unambiguous electron density for the bound inhibitor. The x-ray data collection and crystallographic refinement statistics for these three structures are presented in Table I. The coordinates have been deposited in the Protein Data Bank, 1PKG (activated), 1T45 (autoinhibited), and 1T46 (STI-571 co-complex).

Conformational Flexibility Calculations—Coordinate uncertainties were estimated using the B-factor scaled version of Cruickshank's diffraction-component precision index (43), which is based on B-factors including the translation, liberation, and screw-rotation contributions (44). The coordinate uncertainties for the activated conformation ranged from 0.246 to 0.688 Å with a mean of 0.365 ± 0.076 Å. The coordinate uncertainties for the autoinhibited conformation were significantly smaller reflecting the higher resolution of the diffraction data used to refine the structure, values ranged from 0.080 to 0.313 Å with a mean of 0.138 ± 0.048 Å.

RESULTS AND DISCUSSION

Structure of Active c-Kit Kinase—The activated and autoinhibited c-Kit kinase structures were obtained from constructs containing an intact juxtamembrane region (approximately residues from Thr^{544} to Trp^{580}) followed by the kinase domains. The KID is a region of variable length and unknown function that splits the coding sequence for the C-lobe of many RPTKs, and is truncated in these constructs (see "Experimental Procedures"). Crystals of the active c-Kit kinase are obtained by pre-incubating purified protein samples with ATP and Mg^{2+} to initiate the *trans* autophosphorylation reaction. Analysis of the reaction products by mass spectrometry (37) shows that the primary sites of phosphorylation are Tyr^{568} and Tyr^{570}, which are located near the junction of the juxtamembrane domain and the N-lobe of the kinase (Fig. 1*B*). The x-ray data collection and 2.65-Å resolution refinement statistics for activated c-Kit are presented in Table I. This structure contains two c-Kit enzyme molecules in the crystallographic asymmetric unit, with phosphotyrosine (PTR)-568 from the amino termini of adjacent molecules in the crystal lattice binding in *trans* at the

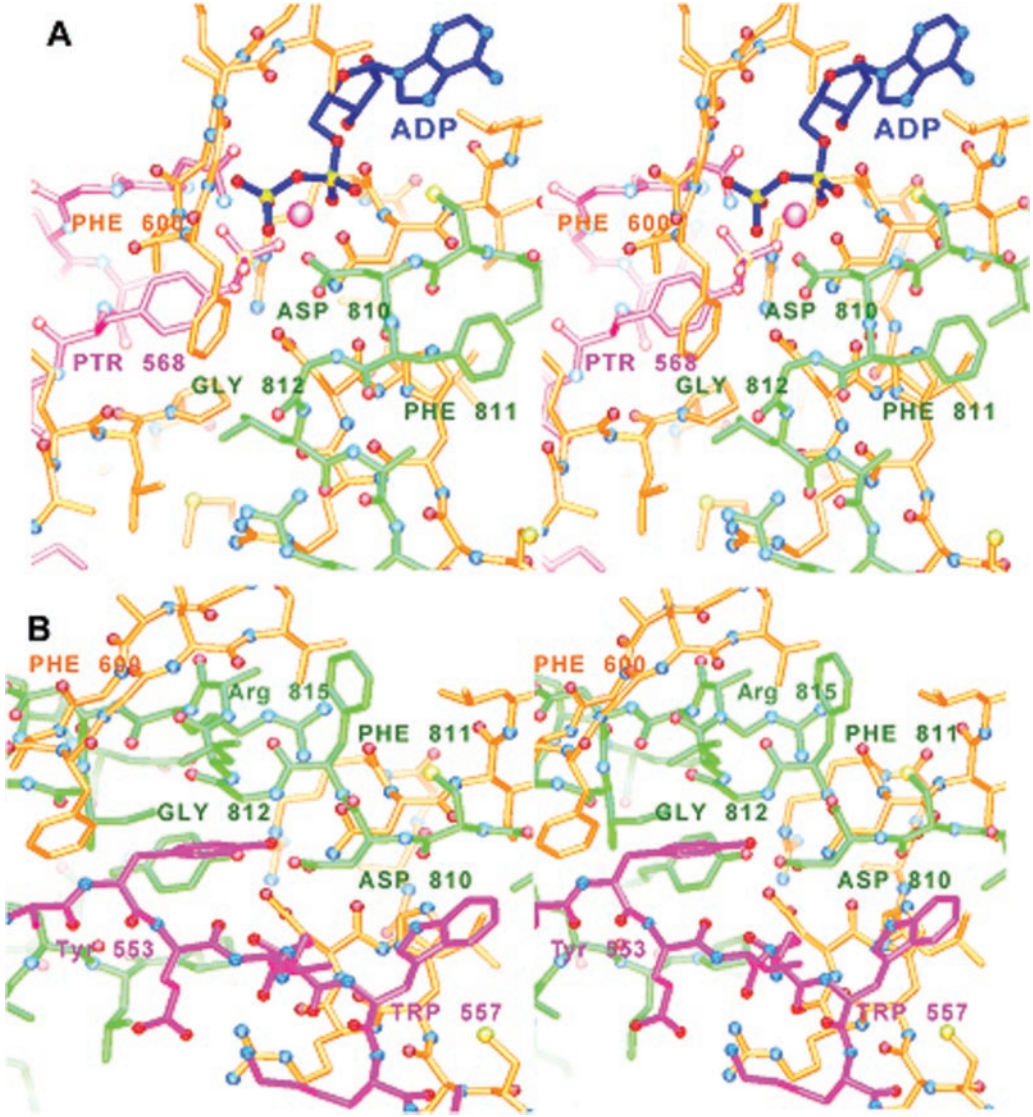

FIG. 3. **On and off conformations of the c-Kit kinase A-loop DFG motif.** *A*, stereo view of the nucleotide-bound c-Kit kinase-active center. The DFG motif (Asp^{810}, Phe^{811}, Gly^{812}) is in a conformation that allows nucleotide binding with Asp^{810} ligating the bound Mg^{2+} ion (*pink sphere*). In this product complex structure, the P-loop (*orange*) with Phe^{600} shields the active center, and the γ-phosphate group of ATP has been transferred to the target tyrosine residue PTR-568. *B*, stereo view of the autoinhibited c-Kit kinase-active center. The penetration of the autoinhibitory juxtamembrane region (*purple*) inserts Trp^{557} into the area that Phe^{811} occupies in the activated structure. The DFG motif is in the autoinhibited off state with Phe^{811} flipped over and occluding the nucleotide binding site. In this pseudosubstrate complex, The A-loop (*green*) is folded back and the P-loop (*orange*, *upper left*) is shifted from its nucleotide-bound position.

kinase-active center. In the active c-Kit kinase structure, the ~20 amino acid residues of the juxtamembrane domain preceding Tyr^{568} (Fig. 1*B*) of both enzymes in the crystallographic asymmetric unit are disordered as are the residues of the truncated KID.

The structure of active c-Kit kinase domain is consistent with the common protein kinase fold (Fig. 2*A*). The smaller N-lobe is comprised of mostly β-strands and a single α-helix, the C-helix, that modulates activity via contacts with the nucleotide binding site and DFG motif at the base of the activation loop (A-loop) (Fig. 2, *A* and *B*). Residue Glu^{640} of the C-helix of active c-Kit provides a critical salt link to the buried side chain of Lys^{623}, which bridges the α- and β-phosphates of the bound ADP. The c-Kit DFG motif is also in an active conformation, with Asp^{810} coordinating the Mg^{2+} ion bridging the α- and β-phosphates, and Phe^{811} positioned to allow binding of the adenine moiety of the nucleotide (Fig. 3*A*).

The active c-Kit kinase enzyme structure is a product complex, with ADP, a Mg^{2+} ion, and the side chain of PTR-568 bound at the kinase-active site. As PTR-568 is covalently attached to another enzyme molecule in the crystal, substrate peptide binding in *trans* is restricted by crystal packing interactions. Although the details of phosphotyrosine binding at the active center is identical in both molecules of the asymmetric unit, the global course of the substrate peptide binding differs. We have focused our discussion on substrate peptide binding to molecule A, as in this configuration the peptide packs against and stabilizes the active conformation of the A-loop (37). The activation loop is in the active conformation, despite the fact that the target A-loop tyrosine, Tyr^{823}, is not phosphorylated. The side chain of Tyr^{823} is directed toward a positively charged region formed by the guanidinium groups of Arg^{815} and Arg^{791}. A PTR residue at this position would further stabilize the kinase A-loop in an active conformation.

Structure of Autoinhibited c-Kit Kinase—Many protein kinases are maintained in an inactive state in the absence of activating signals, a fact first determined for the Ser/Thr protein kinases (45), and recently observed for the protein-tyrosine kinases (46). For many non-receptor tyrosine kinases, such as the Abl kinase, the inactive state of the kinase is maintained

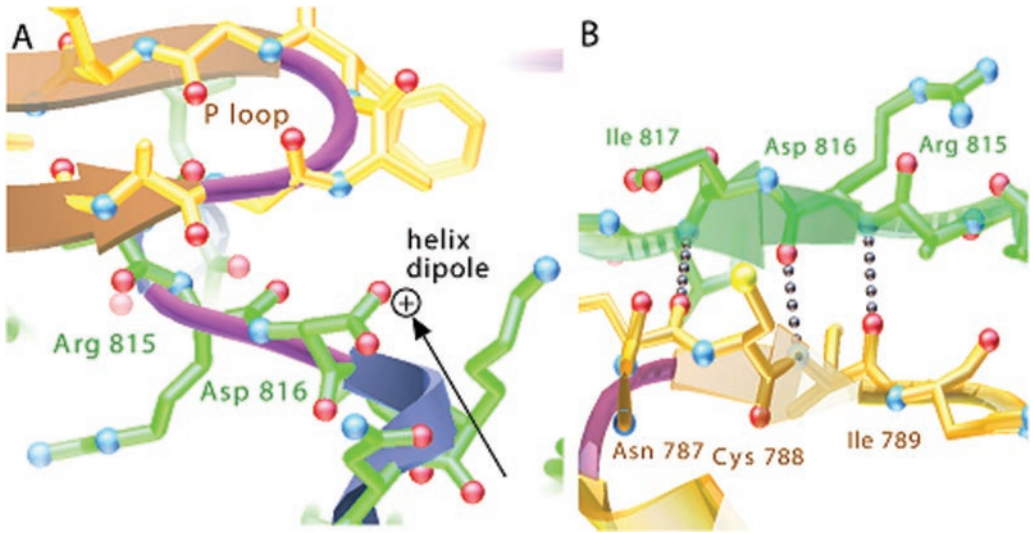

FIG. 4. **The structure and environment surrounding the frequently mutated residue Asp^{816} in the autoinhibited and activated c-Kit kinase structures.** *A*, view of the structural environment surrounding Asp^{816} in the autoinhibited kinase structure. Asp^{816} is situated between the P-loop and a short region of 3_{10} helix where the negatively charged Asp side chain can stabilize the positively charged helical dipole. *B*, view of the structural environment surrounding Asp^{816} in the activated kinase structure. Arg^{815} and Ile^{817} form β-sheet hydrogen bonding interactions with Ile^{79} and Asn^{787} of the C-lobe to stabilize the activation loop in an extended conformation.

through SH2 and SH3 protein interaction domains that associate with and inhibit the kinase domain (47). The RPTKs, such as c-Kit, lack these inhibitory protein interaction domains, and the kinase is activated via ligand-mediated receptor dimerization. In addition to its role as a substrate for *trans* autophosphorylation *in vivo*, there is compelling evidence that the juxtamembrane domain of the Type III RPTKs also functions as an autoinhibitory domain. Unfortunately, much of this region is disordered in the active structure of c-Kit. The structure of autoinhibited c-Kit kinase, which has an ordered juxtamembrane domain, permits the dual function of the juxtamembrane region to be more clearly understood.

The structure of c-Kit in an autoinhibited conformation was determined using the active c-Kit kinase domain structure as a molecular replacement search model. Even at the earliest stages of refinement the electron density maps indicated that a substantial rearrangement and shifting of the structural elements in the kinase N-lobe had occurred (Fig. 2*B*). The high resolution 1.90-Å data for the autoinhibited structure allowed for the entire polypeptide chain to be fit unambiguously, including the residues for the truncated KID and the amino-terminal residues that were not visible in the activated kinase structure.

Contrary to the possibility that the Type III RPTK juxtamembrane regions might adopt a "WW-like" β-sheet domain (24) or an α-helical structure (23), the juxtamembrane domain forms a compact hairpin loop that inserts directly into the domain interface between the kinase N- and C-lobes (Fig. 2*B*). The ~20 amino-terminal residues of the juxtamembrane domain, from Tyr^{547} to Gly^{565}, comprise the inner buried half of this hairpin loop and form specific interactions that disrupt the conformation of the kinase DFG motif and A-loop (see below). The subsequent region that contains the target tyrosine residues of the autophosphorylation reaction extends along the exterior solvent-exposed half of the hairpin loop (Fig. 2*B*). Juxtamembrane region residues identified by site-directed mutagenesis as critical in maintaining the autoinhibited state (Fig. 2) make important interactions in the interface between the amino-terminal autoinhibitory domain and the formal kinase N- and C-lobes (Fig. 3*B*). The side chains of Val^{559} and Val^{560} stabilize a hydrophobic patch formed by Val^{643}, Tyr^{646}, Cys^{788}, and Ile^{789}, whereas Tyr^{553} penetrates deeply into the interface (Fig. 3*B*) and forms hydrogen bonds between its side chain–OH group and the side chains of buried and conserved residues Asp^{810} of the DFG motif and Glu^{640}.

In the active c-Kit kinase structure, the conformation of the polypeptide backbone is such that Phe^{811} of the DFG motif does not block the nucleotide-binding site (Fig. 3*A*). However, in the autoinhibited kinase conformation, Phe^{811} is blocked from this position by Trp^{557} and occludes the active site. (Fig. 3*B*). The kinase DFG motif flips between the "on" and "off" states by rotating about the ϕ main chain torsion angle of Asp^{810}, which maintains the Asp^{810} carboxylate side chain in approximately the same position in the two enzyme conformations. In active c-Kit kinase Asp^{810} ligates the Mg^{2+} ion bound between the nucleotide phosphates, whereas in the autoinhibited state the side chain of Asp^{810} is directed toward the positively charged guanidinium group of Arg^{815}. In the active structure, Arg^{815} forms a hydrogen bond with the Tyr^{823} side chain, which is the key residue within the A-loop that becomes phosphorylated *in vivo*, and this interaction stabilizes the active conformation of the kinase. The D816V and D816H dominant activating mutants (48, 15) may invert the conformation of the protein backbone such that the side chain of residue 816 points inward resulting in the side chain of Arg^{815} being flipped from its position in the autoinhibited structure. Alternatively, the deleterious effects of Asp^{816} substitutions may derive from the ability of this residue to stabilize a small positively charged α-helical dipole by virtue of the negative charge of its side chain. Asp^{816} serves as the amino-terminal capping residue for approximately one turn of α-helix including residues Ile^{817}, Lys^{818}, Asn^{819}, and Asp^{820} (Fig. 4*A*), and a mutation of Asp^{816} to a hydrophobic or aromatic residue would potentially destabilize this helical segment and thereby could alter the entire activation loop toward its activated structure where Asp^{816} is involved in a β-sheet interaction (Fig. 4*B*). A similar helix-capping interaction may also account for the susceptibility toward an activating mutation of an equivalent Aspartic acid residue in the Flt-3 kinase.

The Activation Loop Binds as a Pseudosubstrate in the Autoinhibited Structure—The structural switch of the kinase DFG motif alters the course of the c-Kit activation loop, which folds back over the C-lobe relative to the extended conformation of the A-loop seen in the active c-Kit structure (Fig. 2). More-

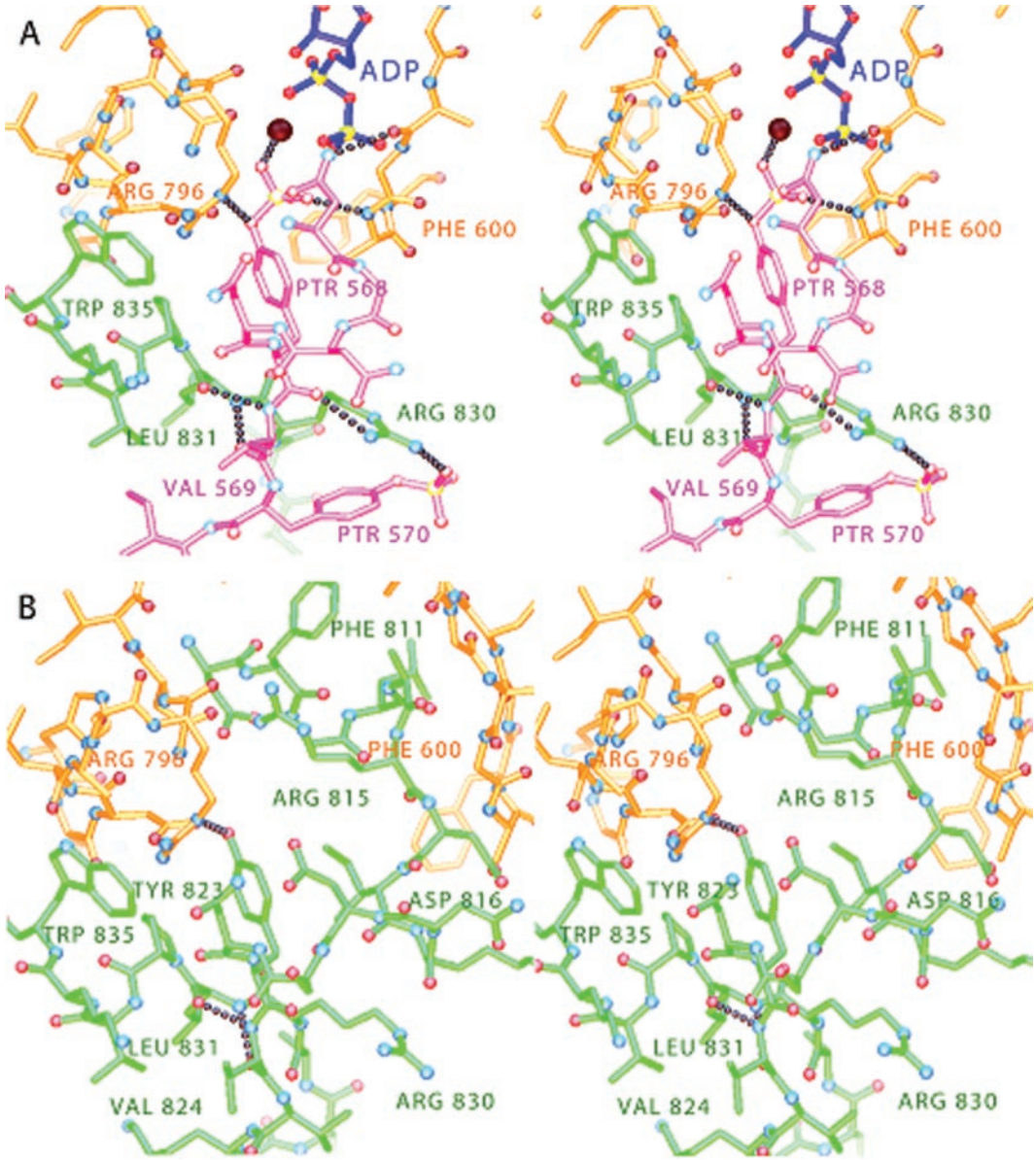

FIG. 5. **Substrate binding and pseudosubstrate autoinhibition of c-Kit kinase.** *A*, stereo view of the product-complex c-Kit structure. The amino-terminal signal peptide (*purple*) from another c-Kit enzyme molecule is bound in *trans*, and phosphotyrosine residue PTR-568 is interacting with bound Mg^{2+} ion (*red sphere*) and conserved residue Arg^{796}. *B*, stereo view of the autoinhibited c-Kit kinase structure. In this pseudosubstrate complex, The A-loop (*green*) is folded back and inserts Tyr^{823} into the position occupied by PTR-568 from the second enzyme molecule in the nucleotide-bound active structure.

over, in the autoinhibited conformation, the amino-terminal portion of the juxtamembrane domain occupies the same region in space where the extended active A-loop would reside, and thus physically blocks the A-loop from attaining an active conformation. In the autoinhibited state, the target A-loop tyrosine, Tyr^{823}, inserts into the kinase-active center and binds as a pseudosubstrate mimicking the interactions seen in the product complex with the phosphotyrosine residue (Fig. 5, *A* and *B*). In this conformation, the side chain of Tyr^{823} packs between Pro^{832} and Ile^{817} and forms hydrogen bonds between its side chain hydroxyl and Asp^{792} Oδ-1 and Arg^{796} Nϵ atoms. Asp^{792} and Arg^{796} are strictly conserved among the Type III RPTKs. For the activated kinase, PTR-568 binds similarly in *trans*, with additional interactions from the phosphate group to Asn^{797} Nδ-2 and the bound Mg^{2+} ion, but the PTR side chain inserts between Pro^{832} and Ala^{599} from the kinase P-loop (Figs. 3*A* and 5*A*). The switching of the kinase DFG motif and consequent structural rearrangement of the autoinhibited A-loop forces the P-loop away from its position in the active structure to a position ~6 Å away in the autoinhibited state (Fig. 3*B*), as measured from the Cα to Cα distance between Phe^{600} in the two superimposed structures. The orientation of the autoinhibited A-loop is similar to the pseudosubstrate-binding orientation first observed in the insulin receptor kinase, IRK (49), and subsequently also in both the structures of c-Abl bound to STI-571 (50) and other compounds (47, 51), the muscle-specific tyrosine kinase, MuSK (33), as well as the recently determined crystal structure of the Flt-3 kinase (52).

This mechanism of kinase autoinhibition by the juxtamembrane domain seen in c-Kit, as well as in the recently determined structure of the related Flt-3 kinase (52), is distinct from that seen in other autoinhibited receptor kinase structures. Notably, the intact juxtamembrane regions of these Type III RPTKs interact extensively with their respective kinase domains disrupting not only the conformation of the critical control C-helix but also physically blocking the kinase DFG motif and A-loop from attaining an active conformation (Figs. 2*B* and 3*B*). Such extensive interactions with key kinase structural

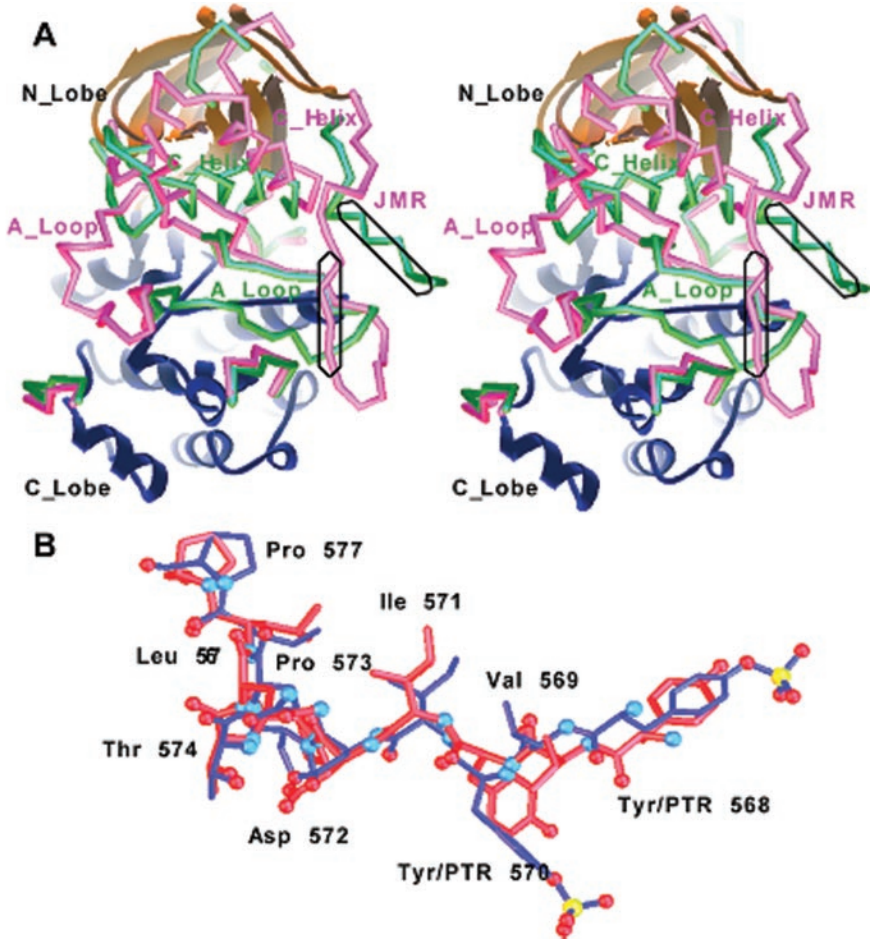

FIG. 6. **Conformational rigidity and flexibility in the autoinhibited to active c-Kit kinase structure transition.** *A*, global conformational flexibility. The autoinhibited and active c-Kit kinase structures are shown superimposed according to their rigid C-lobe α-helical cores (*blue ribbons*). This illustrates the domain rotation of the rigid N-lobe core β-sheet (*gold arrows*). Regions that show significant conformational change, including the A-loop and C-helix, are shown for the autoinhibited (*pink tubes*) and active (*green tubes*) kinase structures. The substrate peptide regions shown superimposed in *B* are *circled*. *B*, local conservation of structure. The portion of the juxtamembrane domain encompassing the substrate tyrosines, Tyr^{568} and Tyr^{570}, are shown locally superimposed for the active (red) and autoinhibited (*blue*) kinase structures. Despite markedly different structural environments this region maintains its local conformation suggesting that this is the preferred substrate peptide conformation for c-Kit *trans* activation *in vivo*.

elements are not generally observed in other autoinhibited kinase structures, such as the EphB2 RPTK where the unphosphorylated juxtamembrane region adopts a helical conformation that specifically interacts with and disrupts only the C-helix of the kinase N-lobe (32). A similar specific disruption of the C-helix is observed by an α-helical juxtamembrane region of the MuSK RPTK (33), whereas the c-Abl non-receptor tyrosine kinase is maintained in an autoinhibited state through interactions mediated by an amino-terminal myristoyl modification and ancillary SH2 and SH3 protein domains. These diverse autoinhibitory mechanisms among different families of receptor tyrosine kinases highlight the complexity and conformational flexibility of protein kinases (46).

Rigidity and Flexibility of the Autoinhibited to Active Kinase Transition—To help examine the transition between the autoinhibited and activated c-Kit kinase structures, the parts of the kinase that are flexible, and the regions that are conformationally invariant were identified by the analysis of error-scaled Cα difference distance matrices (44). The central cores of both the kinase N- and the C-lobes behave as two essentially independent rigid bodies that move with respect to each other in the structural transition (Fig. 6*A*). For the C-lobe, 147 residues (673–689, 766–808, 832–843, 849–871, 876–927) form an independent rigid domain in which Cα atoms superimpose within 0.42-Å root mean square (RMS) deviation in the two structures, whereas for the N-lobe an independent rigid domain is formed by 58 residues (580–594, 602–611, 615–625, 644–650, 655–662, 666–672) that superimpose the Cα atoms within a 0.44-Å RMS deviation. These values are within the range of the coordinate uncertainties for the lower resolution activated structure and compare with an RMS deviation of 1.62 Å when the two structures are superimposed globally. The remaining parts of c-Kit show significant local movements when the protein switches between the autoinhibited and activated forms (Fig. 6A). These conformationally flexible residues include the amino-terminal autoinhibitory domain (residues 547–579), the P-loop (595–601), a peripheral loop in the N-lobe (612–614), the C-helix (626–643), a loop that contacts the C-helix via Arg^{634} in the autoinhibited form (663–665), and a loop of the N-lobe that contacts the C-lobe (651–654). In the C-lobe, these flexible regions include the truncated KID region (690–765), the A-loop (809–831), a small loop in contact with the A-loop (872–875), and a second small loop in the C-lobe that contacts the target tyrosine-containing region of the autoinhibitory domain (844–848).

The local conformation surrounding the substrate portion of the juxtamembrane domain is conserved despite global structural flexibility. The local conformation of this region is remarkably similar to the peptide conformation observed bound in *trans* in the activated structure (Fig. 6*B*), suggesting that no major structural reorganization of the target tyrosine-containing region needs to occur for the *trans* autophosphorylation reaction to proceed *in vivo*. Very recently, Griffith *et al.* (52) reported the structure of the Flt-3 kinase domain and proposed a mechanism for the way in which the juxtamembrane domain regulates kinase activity where the role for the homologous region encompassing from Ile^{557} to Trp^{580} is to maintain and align the substrate tyrosines in the proper register during and after the transition from autoinhibited to activated structure (52). Our c-Kit structures allow a direct comparison of this region and indicate that it maintains the substrate in a favorable conformation for binding to another kinase in *trans*, whereas the length of this region is strictly conserved among

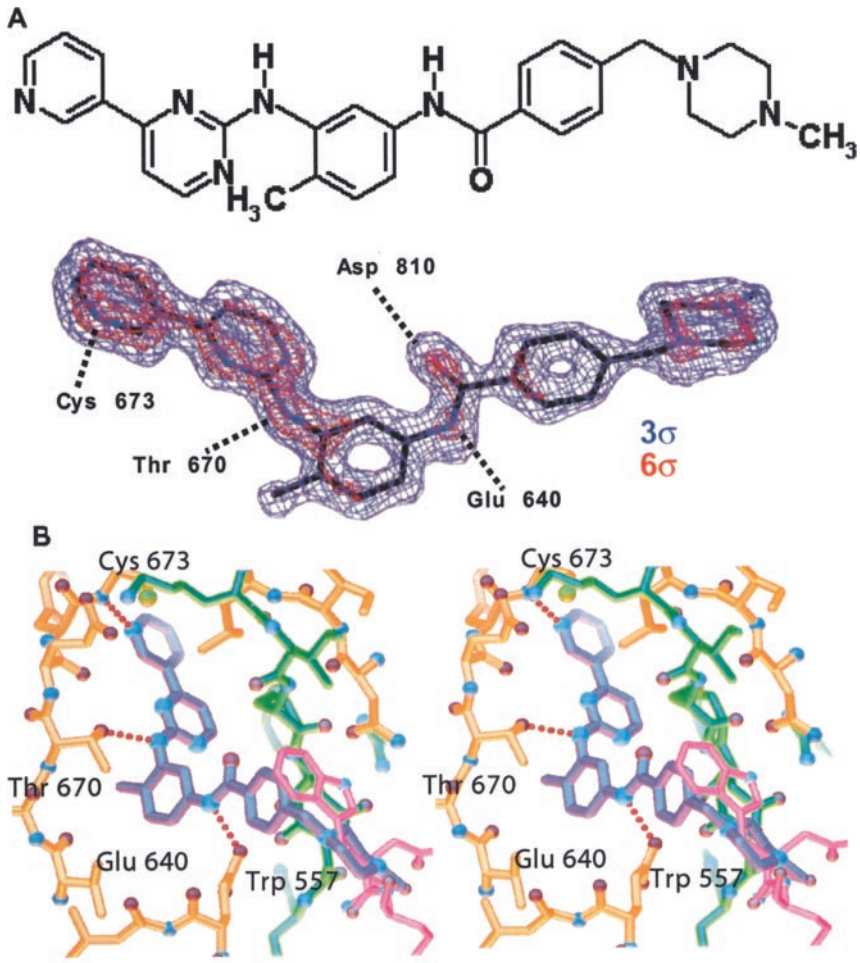

FIG. 7. **STI-571 binding and interactions with c-Kit kinase.** *A*, chemical structure of STI-571 and $F_{obs} - F_{calc}$ omit difference electron density calculated prior to building the inhibitor into the co-crystal structure, contoured at 3σ (*blue*) and 6σ (*red*). Key hydrogen bonds are depicted. *B*, stereo view of STI-571 (*purple*) binding to c-Kit showing key hydrogen bonds formed with the hinge residue Cys^{673}, gatekeeper residue Thr^{670}, and conserved residue Glu^{640}. The polypeptide surrounding Trp^{557} from the virgin autoinhibited c-Kit structure is shown superimposed on the STI-571 complex structure.

the Type III RPTKs to ensure that self-activation via *cis* autophosphorylation cannot occur.

STI-571 Co-crystal Structure and Implications for c-Kit Inhibition—RPTKs occupy a position at the top of cellular growth and proliferation signal transduction cascades, and their aberrant activation is often implicated in human disease. RPTKs thus are attractive targets for therapeutic intervention by small molecule inhibitors. Many of these inhibitors are competitive with ATP, binding at the conserved kinase nucleotide-binding site, and are often targeted to the active kinase conformation. Specificity for particular kinases can be achieved by exploiting small sequence and conformational variations surrounding the ATP-binding pocket. Drugs that target distinct inactive kinase conformations, however, are likely to attain a greater degree of specificity. One such successful drug compound is STI-571, which is an effective treatment for chronic myelogenous leukemia by specifically targeting the Abl kinase. STI-571 does not inhibit the Ser/Thr protein kinases, nor many of the tyrosine kinases, including Flt-3, but it is an effective inhibitor of platelet-derived growth factor and c-Kit (36), the two closely related Type III RPTKs.

Unlike crystal structures of the Abl kinase, our autoinhibited c-Kit kinase structure is obtained in the absence of any bound inhibitor and is thus proof that this protein conformation exists independently and is not induced by STI-571 binding. Furthermore, our autoinhibited structure indicates that STI-571 is not an ideal compound for maintaining c-Kit in the autoinhibited state. STI-571 consists of a 2-phenylaminopyrimidine core plus a pyridine linked via a peptide bond to a phenyl ring and a piperazinyl group (Fig. 7*A*). Our c-Kit kinase autoinhibited structure suggests that STI-571 is too large to fit within the pocket formed at the N- and C-lobe interface of the autoinhibited structure (Fig. 7*B*). To test this hypothesis, we performed proteolysis experiments with and without added inhibitor. The protein is resistant to protease cleavage in the absence of added STI-571 but is cleaved readily when STI-571 is added in a molar excess (data not shown), providing evidence that STI-571 binding to c-Kit actually disrupts the autoinhibitory domain. This protease-treated c-Kit protein was crystallized and the co-crystal structure of a c-Kit·STI-571 complex solved and refined to a 1.6-Å resolution (Table I).

STI-571 binds to autoinhibited c-Kit in a similar manner to that observed in the complex with the Abl kinase (51); however there is an induced readjustment of the DFG motif because of a steric clash with the side chain of Phe^{810} (Fig. 7*B*). Many small molecule inhibitors of protein kinases mimic the interactions made with the adenine portion of ATP, inserting into the cleft between the kinase N- and C-lobes and forming hydrogen bonds to the polypeptide backbone of hinge region residues. Although there is a slight tilt of the aminopyrimidine and pyridine rings of STI-571 bound to c-Kit as compared with Abl, the hydrogen-bonding interactions are similar, with a 2.85-Å hydrogen bond between the pyridine nitrogen and the backbone amide of c-Kit residue Cys^{673} and a 2.95-Å hydrogen bond formed between the aminopyrimidine nitrogen of STI-571 and the side chain Oγ-1 atom of the gatekeeper residue Thr^{670} (Fig. 7*B*). Active kinase structures are characterized by a critical salt link between a conserved C-helix glutamic acid residue and a lysine residue that orients the lysine side chain for interaction with the nucleotide phosphates. This salt link (~2.7 Å) between Glu^{640} and Lys^{623} is maintained in autoinhibited c-Kit, with the Oϵ-1 atom of Glu^{640} also forming a 2.8-Å hydrogen bond

with the nitrogen of the STI-571 peptide bond linker. The carbonyl oxygen of the STI-571 peptide bond is within hydrogen-bonding distance (~3.1 Å) of the backbone amide of Asp^{810} in the c-Kit DFG motif. The phenyl ring of STI-571 packs loosely between the aliphatic portions of the side chains of Asp^{810}, Glu^{640}, and the side chain of Leu^{644}, whereas the piperazine ring of the inhibitor makes no specific interactions with the protein but rests in a shallow pocket bounded by Val^{643}, Cys^{788}-Ile^{789}-His^{790}-Arg^{791}, and Asp^{810}. Superimposing our virgin c-Kit autoinhibited structure on the STI-571 complex structure clearly shows that these latter two moieties of STI-571, namely the phenyl and piperazinyl rings, are incompatible with the fully assembled autoinhibited structure of c-Kit kinase. Although STI-571 binding does not necessarily induce the autoinhibited conformation, it does clash with and disrupt the molecular mechanism that has evolved to maintain c-Kit in its off state. By replacing these disruptive portions of STI-571 with shorter chemical entities that actually stabilize the natural autoinhibited state, therapeutic compounds with higher affinities and greater specificity for c-Kit might be developed. By extension such inhibitors could also be effective against the other Type III RPTKs, including platelet-derived growth factor and Flt-3.

Our crystal structures of c-Kit kinase reveal a simple and elegant manner in which the small juxtamembrane domain functions to maintain the kinase in an autoinhibited state. Insertion of this autoinhibitory domain into the cleft between the kinase N- and C-lobes flips the DFG motif into its off state, thereby inducing the activation loop to fold back over from its extended conformation in the active kinase where it binds as a pseudosubstrate at the kinase-active center. A co-crystal structure of c-Kit kinase in complex with the inhibitor STI-571 reveals that this compound binds to the inactive kinase but that STI-571 binding in fact disrupts the mechanism that has evolved to maintain this inactive state through an association of the autoinhibitory juxtamembrane domain with the kinase domains. These results demonstrate that effective inhibitors of the Type III protein-tyrosine kinases could be developed that exploit the unique autoinhibited conformations of these kinases.

Acknowledgments—We thank N. J. Dibb, D. J. Hosfield, Ciarán N. Cronin, and R. A. Wijnands for helpful advice and discussions, W. Joe Rogers for baculovirus expression, Marie Hu for DNA sequencing, and the staff and facilities of the Advanced Light Source (ALS), which is supported by the Director, Office of Science, Office of Basic Energy Sciences, Materials Sciences Division, of the United States Department of Energy under Contract Number DE-AC03-76SF00098 at the Lawrence Berkeley National Laboratory.

REFERENCES

1. Linnekin, D. (1999) *Int. J. of Biochem. Cell Biol.* **31,** 1053–1074
2. Besmer, P., Murphy, J. E., George, P. C., Qiu, F. H., Bergold, P. J., Lederman, L., Snyder, H. W., Jr., Broudeur, D., Zuckerman, E. E., and Hardy, W. D. (1986) *Nature* **320,** 415–421
3. Coussens, L., Van Beveren, C., Smith, D., Chen, E., Mitchell, R. L., Isacke, C. M., Verma, I. M., and Ullrich, A. (1986) *Nature* **320,** 277–280
4. Rosnet, O., Schiff, C., Pebusque, M.-J., Marchetto, S., Tonnelle, C., Toiron, Y., Birg, F., and Birnbaum, D. (1993) *Blood* **82,** 1110–1119
5. Claesson-Welsh, L., Eriksson, A., Westermark, B., and Heldin, C.-H. (1989) *Proc. Natl. Acad. Sci. U. S. A.* **86,** 4917–4921
6. Yarden, Y., Escobedo, J. A., Kuang, W.-J., Yang-Feng, T. L., Daniel, T. O., Tremble, P. M., Chen, E. Y., Ando, M. E., Harkins, R. N., Francke, U., Fried, V. A., Ullrich, A., and Williams, L. T. (1986) *Nature* **323,** 226–232
7. Yarden, Y., Kuang, W.-J., Yang-Feng, T., Coussens, L., Munemitsu, S., Dull, T. J., Chen, E., Schlessinger, J., Francke, U., and Ullrich, A. (1987) *EMBO J.* **6,** 3341–3351
8. Ullrich, A., and Schlessinger, J. (1990) *Cell* **61,** 203–212
9. Heldin, C.-H. (1995) *Cell* **80,** 213–223
10. Hubbard, S. R., Mohammadi, M., and Schlessinger, J. (1998) *J. Biol. Chem.* **273,** 11987–11990
11. Weiss, A., and Schlessinger, J. (1998) *Cell* **94,** 277–280
12. Blume-Jensen, P., and Hunter, T. (2001) *Nature* **411,** 355–365
13. Hirota, S., Isozaki, K., Moriyama, Y., Hashimoto, K., Nishida, T., Ishiguro, S., Kawano, K., Hanada, M., Kurata, A., Takeda, M., Tunio, G. M., Matsuzawa, Y., Kanakura, Y., Sinomura, Y., and Kitamura, Y. (1998) *Science* **279,** 577–580
14. Nishida, T., Hirota, S., Taniguchi, M., Hashimoto, K., Isozaki, K., Nakamura, H., Kanakura, Y., Tanaka, T., Takabayashi, A., Matsuda, H., and Kitamura, Y. (1998) *Nat. Genet.* **19,** 323–324
15. Tian, Q., Frierson, H. F., Jr., Krystal, G. W., and Moskaluk, C. A. (1999) *Am. J. Pathol.* **154,** 1643–1647
16. Kitamura, Y., Hirota, S., and Nishida, T. (2001) *Mutat. Res.* **477,** 165–171
17. Longley, B. J., Jr., Metcalfe, D. D., Tharp, M., Wang, X., Tyrrell, L., Lu, S.-Z., Heitjan, D., and Ma, Y. (1999) *Proc. Natl. Acad. Sci. U. S. A.* **96,** 1609–1614
18. Frost, M. J., Ferrao, P. T., Hughes, T. P., and Ashman, L. K. (2002) *Mol. Cancer Ther.* **12,** 1115–1124
19. Ma, Y., Zeng, S., Metcalfe, D. D., Akin, C., Dimitrijevic, S., Butterfield, J. H., McMahon, G., and Longley, B. J. (2002) *Blood* **99,** 1741–1744
20. Ueda, S., Ikeda, H., Mizuki, M., Ishiko, J., Matsumura, I., Tanaka, H., Shibayama, H., Sugahara, H., Takai, E., Zhang, X., Machii, T., and Kanakura, Y. (2002) *Int. J. Hematol.* **76,** 427–435
21. Zermati, Y., De Sepulveda, P., Feger, F., Letard, S., Kersual, J., Casteran, N., Gorochev, G., Dy, M., Ribadeau Dumas, A., Dorgham, K., Parizot, C., Bieche, Y., Vidaud, M., Lortholary, O., Arock, M., Hermine, O., and Dubreuil, P. (2003) *Oncogene* **22,** 660–664
22. Kozlowski, M., Larose, L., Lee, F., Le, D. M., Rottapel, R., and Siminovitch, K. A. (1998) *Mol. Cell. Biol.* **18,** 2089–2099
23. Ma, Y., Cunningham, M. E., Wang, X., Ghosh, I., Regan, L., and Longley, B. J. (1999) *J. Biol. Chem.* **274,** 13399–13402
24. Irusta, P. M., and DiMaio, D. (1998) *EMBO J.* **17,** 6912–6923
25. Irusta, P. M., Luo, Y., Bakht, O., Lai, C.-C., Smith, S. O., and DiMaio, D. (2002) *J. Biol. Chem.* **277,** 38627–38634
26. Ilsley, J. L., Sudol, M., and Winder, S. J. (2002) *Cell. Signal.* **14,** 183–189
27. Macias, M. J., Wiesner, S., and Sudol, M. (2002) *FEBS Lett.* **513,** 30–37
28. Sudol, M., and Hunter, T. (2000) *Cell* **103,** 1001–1004
29. Chan, P. M., Ilangumaran, S., La Rose, J., Chakrabartty, A., and Rottapel, R. (2003) *Mol. Cell. Biol.* **23,** 3067–3078
30. Hubbard, S. R., and Hill, J. H. (2000) *Annu. Rev. Biochem.* **69,** 373–398
31. Hubbard, S. R. (2002) *Curr. Opin. Struct. Biol.* **12,** 735–741
32. Wybenga-Groot, L. E., Baskin, B., Ong, S. H., Tong, J., Pawson, T., and Sicheri, F. (2001) *Cell* **106,** 745–757
33. Till, J. H., Becerra, M., Watty, A., Lu, Y., Ma, Y., Neubert, T. A., Burden, S. J., and Hubbard, S. R. (2002) *Structure* **10,** 1187–1196
34. Li, S., Covino, N. D., Stein, E. G., Till, J. H., and Hubbard, S. R. (2003) *J. Biol. Chem.* **278,** 26007–26014
35. O'Dwyer, M. E., Mauro, M. J, and Druker, B. J. (2003) *Cancer Investig.* **3,** 429–438
36. Buchdunger, E., Cioffi, C. L., Law, N., Stover, D., Ohno-Jones, S., Druker, B. J., and Lydon, N. B. (2000) *J. Pharmacol. Exp. Ther.* **295,** 139–145
37. Mol, C. D., Lim, K. B., Sridhar, V., Zou, H., Chien, E. Y., Sang, B.-C., Nowakowski, J., Kassel, D. B., Cronin, C. N., and Mcree, D. E. (2003) *J. Biol. Chem.* **278,** 31461–31464
38. Hosfield, D., Palan, J., Hilgers, M., Scheibe, D., McRee, D. E., and Stevens, R. C. (2003) *J. Struct. Biol.* **142,** 207–217
39. Otwinowski, Z., and Minor, W. (1997) *Methods Enzymol.* **276,** 307–326
40. Navaza, J. (2001) *Acta Crystallogr. Sect. D* **57,** 1367–1372
41. Murshudov, G. N., Vagin, A. A., and E. J. Dodson. (1997) *Acta Crystallogr. Sect. D* **53,** 240–255
42. McRee, D. E. (1999) *J. Struct. Biol.* **125,** 156–165
43. Cruickshank, D. W. (1999) *Acta Crystallogr. Sect. D* **55,** 583–601
44. Schneider, T. R. (2002) *Acta Crystallogr. Sect. D* **58,** 195–208
45. Kemp, B. E., and Pearson, R. B. (1991) *Biochim. Biophys. Acta* **1094,** 67–76
46. Huse, M., and Kuriyan, J. (2002) *Cell* **109,** 275–282
47. Nagar, B., Hantschel, O., Young, M. A., Scheffzek, K., Veach, D., Bornmann, W., Clarkson, B., Superti-Furga, G., and Kuriyan, J. (2003) *Cell* **112,** 859–871
48. Piao, X., Paulson, R., van der Greer, P., Pawson, T., and Bernstein, A. (1996) *Proc. Natl. Acad. Sci. U. S. A.* **93,** 14665–14669
49. Hubbard, S. R., Wei, L., Ellis, L., and Hendrickson, W. A. (1994) *Nature* **372,** 746–754
50. Schindler, T., Bornmann, W. G., Pellicena, P., Miller, W. T., Clarkson, B., and Kuriyan, J. (2000) *Science* **289,** 1938–1942
51. Nagar, B., Bornmann, W. G., Pellicena, P., Schindler, T., Veach, D. R., Miller, W. T., Clarkson, B., and Kuriyan, J. (2002) *Cancer Res.* **62,** 4236–4243
52. Griffith, J., Black, J., Faerman, C., Swenson, L., Wynn, M., Lu, F., Lippke, J., and Saxena, K. (2004) *Mol. Cell* **13,** 169–178

Structural Basis for the Autoinhibition and STI-571 Inhibition of c-Kit Tyrosine Kinase

Clifford D. Mol, Douglas R. Dougan, Thomas R. Schneider, Robert J. Skene, Michelle L. Kraus, Daniel N. Scheibe, Gyorgy P. Snell, Hua Zou, Bi-Ching Sang and Keith P. Wilson

J. Biol. Chem. 2004, 279:31655-31663.
doi: 10.1074/jbc.M403319200 originally published online April 29, 2004
